Discrete cosine transform–based local adaptive filtering of images corrupted by nonstationary noise

Vladimir V. Lukin
Dmitriy V. Fevralev
Nikolay N. Ponomarenko
Sergey K. Abramov
National Aerospace University
61070, Kharkov, Ukraine

Oleksiy Pogrebnyak
Instituto Politecnico Nacional
Centro de Investigacion en Computacion
Mexico, DF 07738
olek@pollux.cic.ipn.mx

Karen O. Egiazarian
Jaakko T. Astola
Tampere University of Technology
FIN 33101
Tampere, Finland

Abstract. *In many image-processing applications, observed images are contaminated by a nonstationary noise and no a priori information on noise dependence on local mean or about local properties of noise statistics is available. In order to remove such a noise, a locally adaptive filter has to be applied. We study a locally adaptive filter based on evaluation of image local activity in a "blind" manner and on discrete cosine transform computed in overlapping blocks. Two mechanisms of local adaptation are proposed and applied. The first mechanism takes into account local estimates of noise standard deviation while the second one exploits discrimination of homogeneous and heterogeneous image regions by adaptive threshold setting. The designed filter performance is tested for simulated data as well as for real-life remote-sensing and maritime radar images. Recommendations concerning filter parameter setting are provided. An area of applicability of the proposed filter is defined.*
 [DOI: 10.1117/1.3421973]

1 Introduction

Nowadays, a great number of image filters intended for removal of noise of a given type exists (e.g., for additive,[1] Poisson,[2] speckle,[3] and impulse[4] noise). Other filters are capable to remove different types of mixed noise, such as additive and impulsive,[5,6] multiplicative and impulsive,[7] multiplicative and additive,[8] etc., under assumption that a mixed noise type and its basic parameters are known in advance or preestimated. In order to perform filtering in an efficient way, one has to have a preliminary knowledge on noise type and statistics.[5,9,10] On the other hand, such *a priori* information may not always be available in many typical practical situations that often arise in remote sensing, hyperspectral imaging, ultrasound medical diagnostics, cDNA imaging, etc.[11–15]

For many imaging systems, noise is not a stationary process and its statistics and properties could be quite dissimilar in different fragments of a particular image. In practice, dissimilarities in noise statistics can be due to several basic reasons. One reason is the change of imaging conditions or considerably different distances to particular parts of an observed scene as in side-look radar imaging.[16] Another reason could be uncontrollable influence of several different sources of noise. For instance, in maritime radars, interference arises due to sea clutter that depends on wind speed, direction of sea waves, incidence angle,[16] etc. A third reason could be nonlinear amplification regulations in input circuits before image digitalization as in ultrasound medical devices. Finally, for some imaging systems, adequate models of noise present in the acquired or transferred images have not been established or commonly accepted yet.[17–20]

Therefore, there are typical and atypical situations concerning properties of noise present in images. Typical situations considered thoroughly in image-filtering literature are characterized by the following: noise type is known or its characteristics are known *a priori* or can be estimated for a given type of noise. On the contrary, less-studied situations addressed in this paper are the following:

1. Noise is nonstationary in the sense that its basic characteristics [variance, probability density function in

Paper 09123PRR received Jul. 11, 2009; revised manuscript received Mar. 19, 2010; accepted for publication Mar. 19, 2010; published online May 3, 2010.

1017-9909/2010/19(2)/023007/15/$25.00 © 2010 SPIE and IS&T.

some limits] vary from one local fragment of an image to another fragment.
2. These variations do not have some predictable dependence on local mean as this takes place for (e.g., film-grain or Poisson noise; a simple example of such unpredictable variation could be linear dependence of noise variance on pixel coordinates for one or both axes of an image).

Thus, we deal with a problem of image blind denoising.[21] There are several ways to cope with nonstationary noise. A simple way to follow could be applying nonlinear nonadaptive filters that are robust in wide sense[9,22] (i.e., they do not need and do not take into account any information on the noise statistics). Examples of such filters are standard median, α-trimmed mean, central weighted median, Wilcoxon filters.[9,23] Drawbacks of these filters are well known. Along with noise reduction, these filters can severely distort useful information contained in images.

These shortcomings led to design locally adaptive filters (see Refs. 7, 18, and 24–26 and references therein), including several approaches that employ partial differential equations, anisotropic diffusion, and total variation minimization.[27–29] They have demonstrated considerable improvement of performance in comparison to nonadaptive nonlinear filters due to exploiting different mechanisms of adaptation to image local content. However, some of them (e.g., Refs. 18, 24, and 25), require *a priori* information on noise type and statistics, other ones are rather complicated.

There are also many techniques that perform adaptive filtering in the domain of an orthogonal transform. To name a few, let us mention discrete wavelet transform and discrete cosine transform (DCT)–based filters for the additive noise case,[1,30–32] different filters designed for speckle removal,[3,33,34] and other types of noise.[2,35–37] However, for most of these filters, it is supposed that noise type is known and its parameters are either known in advance or preestimated with appropriate accuracy by preliminary "global" analysis of an image at hand.[36,38]

If noise statistics is unknown and noise is nonstationary, the following set of questions arises:

1. What can serve as a basis for transform-based locally adaptive filtering of images corrupted by nonstationary noise?
2. What can be mechanisms of local adaptation?
3. How accurate can be local estimates of noise statistics and how this accuracy can influence a filter performance?
4. What methods of local estimation of noise statistics are worth applying?

In our opinion, one answer to the first question could be DCT-based filtering. There are several reasons for this. First, DCT-based filtering is usually applied locally, in blocks of fixed[24,31,33,37] or adaptively selected shape and size.[36] Second, DCT-based filtering can be easily adapted to *a priori* known or preestimated noise statistics. DCT-based filters have been earlier proposed and successfully tested for removing multiplicative, Poisson, film-grain, and, in general, signal-dependent noise.[2,24,31,33,37] These filters use an estimate of a local mean in an image block for determining noise local variance and setting a local threshold for hard or soft thresholding of DCT coefficients. Third, DCT-based filtering provides excellent noise suppression in homogeneous image regions,[31] appropriate texture preservation,[24] and good preservation of edges and fine details. Thus, the goal of this paper is to design and test DCT filter modifications applicable to processing images corrupted by nonstationary noise.

The paper is organized as follows. In Section 2, basic principles of DCT-based filtering are described. Main advantages of this approach are mentioned and demonstrated. The ways how to adapt this technique to signal-dependent noise are shown. Section 3 deals with description of two proposed modifications of locally adaptive DCT-based filter. Preliminary testing for simulated images and noise is carried out in Section 4, which also contains data for comparison of the designed methods performance to one of the state-of-the-art methods. Limitations of the method for spatially correlated noise are demonstrated. Real-life image-processing examples are given in Section 5. Finally, we draw conclusions and present possible directions of future work.

2 Basic Principles of Adaptive DCT-Based Filtering

All methods of transform-based signal-image-filtering (denoising) rely on the same basic assumption that a signal in transform domain has more sparse representation than noise.[30,33,35–40] Then, if a component in orthogonal transform domain has a rather large absolute value, it most probably corresponds to information content and should be preserved. If a component has amplitude close to zero (less than a threshold), then it most probably relates to noise and has to be removed (suppressed). Then, filtering can be performed using different orthogonal transforms (wavelets, discrete cosine, Haar, etc.). A choice of basis functions as well as filtering efficiency depend on how high are energy compaction properties of a transform for a given signal (image).

The Karhunen–Loeve transform possesses the best signal decorrelation property in least-squares terms.[41,42] Unfortunately, its coefficients are data dependent and, thus, no fast algorithm of the Karhunen–Loeve transform exists. DCT is almost as efficient as the Karhunen-Loeve transform in terms of signal decorrelation and energy compaction, especially in the case of signals modeled by Markov processes.[41,42] There are also fast algorithms for calculating the DCT.[42,43] Because of these properties, DCT is widely used in image and video compression.[44,45]

Let us recall an operation principle of DCT-based denoising.[31,33,37,42] In general form, the two-dimensional DCT coefficients of an $N_1 \times N_2$ matrix $\mathbf{A}$ may be defined as

$$D(u,v) = c(u)c(v)\sum_{n_1=0}^{N_1-1}\sum_{n_2=0}^{N_2-1}\mathbf{A}(n_1,n_2)\cos\left[\frac{(2n_1+1)u\pi}{2N_1}\right] \times\cos\left[\frac{(2n_2+1)v\pi}{2N_2}\right], \quad (1)$$

where

$$\mu = 0,1,\ldots,N_1-1, \quad v = 0,1,\ldots,N_2-1,$$

$$c(u)=\begin{cases}\dfrac{1}{\sqrt{N_1}}, & u=0\\ \sqrt{\dfrac{2}{N_1}} & 1\leq u\leq N_1-1\end{cases},$$

$$c(v)=\begin{cases}\dfrac{1}{\sqrt{N_2}}, & v=0\\ \sqrt{\dfrac{2}{N_2}} & 1\leq v\leq N_2-1\end{cases}.$$

The standard scalar (2-D) DCT-based denoising operates in square-shaped blocks of a fixed size $N\times N$ and comprises the following steps.[31,37] At the first step, the DCT is performed for each image block with values $\{I_{qs}$: $q=n,n+1,\ldots,n+N-1$, $s=m,m+1,\ldots,m+N-1\}$, to obtain the local spectrum $\{D(k,l,n,m)$: $k=1,2,\ldots,N$, $l=1,2,\ldots,N\}$. The left upper corner of the image block is located at (n,m) and the indices k and l relate to the DCT (spectral) coefficients. At the second step, a thresholding of the coefficients $\{D(k,l,n,m)\}$ is carried out for $k=1,2,\ldots,N$, $l=1,2,\ldots,N$. It is possible to apply either soft or hard thresholding.[37] In this paper, we have applied the hard thresholding of DCT coefficients for image filtering. According to that, the spectral coefficient $D(k,l,n,m)$ remains unchanged if its absolute value is larger than a predefined threshold $T(k,l,n,m)$; otherwise, it is set to zero. The coefficient $D(1,1,n,m)$, which corresponds to the block mean, is not subjected to the thresholding.

After the thresholding, the set of changed coefficients $\{D_T(k,l,n,m)$: $k=1,2,\ldots,N$, $l=1,2,\ldots,N\}$ is obtained for each image block defined by the indices n and m. Next, the inverse DCT is applied to each block of thresholded coefficients and the preliminary filtered image values $I_{\mathrm{pf}}(q,s,n,m)$ are obtained for $q=n,n+1,\ldots,n+N-1$, $s=m,m+1,\ldots,m+N-1$. Because now almost all image pixels belong to $N\times N$ different image blocks, we have for each image pixel (q_o,s_o) usually $N\times N$ preliminary filtered pixel values $I_{\mathrm{pf}}(q_o,s_o,n,m)$, where $n=q_o,q_o-1,\ldots,q_o-N+1$ and $m=s_o,s_o-1,\ldots,s_o-N+1$. Only the pixels near the image borders are exceptions because, for them, the number of such output estimates is smaller (minimally, one for all four image corners).

Then, at the last step, all output estimates for each pixel must be combined in order to obtain the final filtered image I_{f}. The simplest way to do this is to average these estimates. The resulting value for the pixel (q_o,s_o) is then

$$I_{\mathrm{f}}(q_o,s_o)=\frac{1}{N\times N}\sum_{n=q_o-N+1}^{q_o}\sum_{m=s_o-N+1}^{s_o}I_{\mathrm{pf}}(q_o,s_o,n,m). \quad (2)$$

Partial overlapping of blocks can be used to accelerate processing, but it results in less-efficient filtering.[31] For this reason, we exploit fully overlapping blocks.

A threshold $T(k,l,n,m)$ may vary, depending on spatial coordinates defined by indices n and m, or may be frequency dependent[46] in the case when noise is spatially correlated with known or preestimated spatial correlation characteristics. We assume that there is no *a priori* information about noise spatial correlation. Thus, we consider only threshold dependence on n and m.

Concerning the potential of DCT-based filtering with fully overlapping blocks, we would like to recall that it provides performance (in terms of output MSE or PSNR) better or comparable to the best wavelet-based denoising techniques for pure additive and pure multiplicative noise cases.[31,33] Furthermore, the main advantage of DCT-based filtering for the considered case of nonstationary noise is that, being carried out blockwise, it can be easily adapted to local statistical properties of noise.[33,47] To show how this can be done, let us consider the following two image models. The first one is a the case of film grain noise for which a general observation model is

$$I_{qs}=I_{qs}^{\mathrm{tr}}+(I_{qs}^{\mathrm{tr}})^{\gamma}\cdot n_{qs}, \quad (3)$$

where I_{qs}, I_{qs}^{tr}, and n_{qs} denote the noisy image sample (pixel) value, true image value, and signal independent noise component, which is characterized by the variance σ_n^2, respectively, for the qs'th sample, γ is a parameter of film grain noise. Then[33] for an nm'th block, the threshold is set as

$$T(n,m)=\beta[\hat{I}(n,m)], \quad (4)$$

where $\hat{I}(n,m)$ is the estimate of the local mean for the block and the coefficient β controls the threshold value. Usually, β is set approximately equal to 2.6;[31,33] although for better preservation of texture, it is expedient to apply $\beta<2.6$.[24]

Let us confirm this fact with two examples. Figure 1 presents the plots of output MSE on β for the DCT filter described above (8×8 pixel blocks with full overlapping). These plots have been obtained for two standard test images (Lenna and Baboon) corrupted by additive white Gaussian noise [$\gamma=0$ in Eq. (3)] with variances $\sigma_n^2=50$ and $\sigma_n^2=100$, and by Poisson noise. In the former case, $T(n,m)$ is set as $\beta\sigma_n$. In the latter case, $T(n,m)=\beta[\hat{I}(n,m)]^{1/2}$.

As it is seen, all dependencies have minimums that are observed for β of ~2.6 for the image Lenna and ~2.3 for the image Baboon. For other standard test images (Goldhill, Peppers, Barbara) minimums are observed for β approximately equal to 2.6. Similar to other filtering algorithms, noise suppression is less efficient if a processed image has a more complex structure and/or the noise variance is smaller. Note that for additive noise with $\sigma_n^2=100$, the values of output peak signal-to-noise ratio (PSNR) provided by the DCT filter with $\beta=2.6$ are equal to 35.40, 34.42, and 34.61 dB for the images Lenna (512×512), Barbara (512×512), and Peppers (256×256), respectively. This is better than for one of the best state-of-the-art Kervrann's filter (see Ref. 26, Table IV, PSNR=35.18, 33.79, and 34.07 dB, respectively).

Thus, DCT-based filtering has a high potential. However, such performance of the DCT filter is observed under condition of known noise type and statistics. And we are interested in the case of non-stationary noise with unknown characteristics.

As is seen from Eq. (4), the product $\sigma_n[\hat{I}(n,m)]$ is, in fact, an estimate of noise standard deviation (SD) $\hat{\sigma}(n,m)$ in a given block. For $\gamma=0$ (i.e., for pure additive noise),

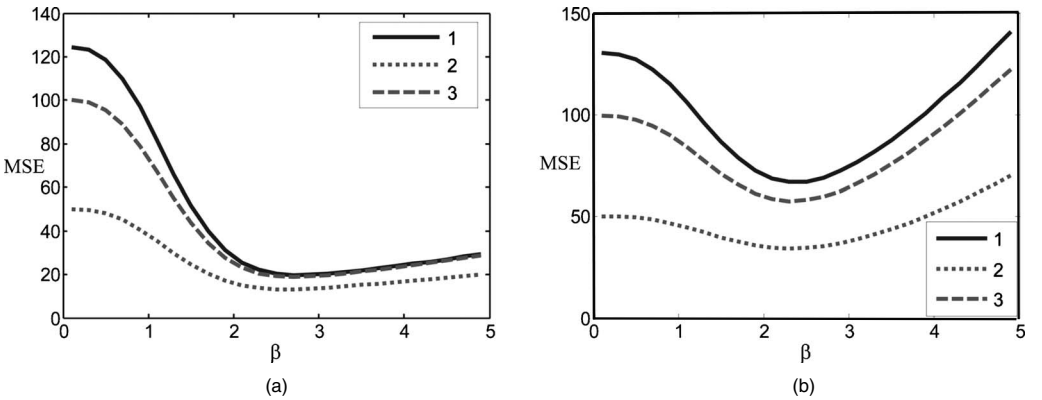

Fig. 1 Output MSE versus β for two standard test images: (a) Lenna and (b) Baboon, corrupted by additive white Gaussian noise with variances 50 (dotted line) and 100 (dashed line) and by Poisson noise (solid line).

one gets exactly σ_n. The threshold is fixed and equal to $\beta\sigma_n$. Similarly, for pure multiplicative case $\hat{\sigma}(n,m) = \sigma_\mu(n,m)\hat{\bar{I}}(n,m)$ where σ_μ is the multiplicative noise normalized SD. As an estimate of local mean $\hat{\bar{I}}(n,m)$, one can use the DCT spectral coefficient $D(1,1,n,m)$.

Thus, generalizing the presented results, the conclusion is as follows. To set a local threshold, one needs a local estimate of noise standard deviation $\hat{\sigma}(n,m)$. Consider the following image additive observation model

$$I_{qs} = I_{qs}^{\mathrm{tr}} + n_{qs}^{\mathrm{nst}}, \tag{5}$$

where I_{qs}^{tr} is a true image value and n_{qs}^{nst} denotes nonstationary noise in a qs'th sample assumed to be zero mean. We suppose that its SD σ_{qs} is a function of pixel coordinates defined by pixel indices qs. It is also assumed that spatial variations of σ_{qs} are not fast, and for a given block, it is possible to assume that nonstationary noise SD is almost constant for all image pixels that belong to a given block. Then, for each block, one needs to have an estimate $\hat{\sigma}(n,m)$. This estimate can be used for setting a local threshold proportionally to $\hat{\sigma}(n,m)$.[39,48]

3 Locally Adaptive DCT Filters

3.1 *DCT Filter Adaptive to Image Local Statistics*

Here, we discuss the fourth question given in Section 1 (i.e., what methods of local estimation of noise statistics can be used). Some initial imagination concerning properties of local estimates of noise variance in blocks or scanning windows with fixed size can be got from earlier studies.[49–52] Generally speaking, noise local SD can be estimated in the spatial or spectral domain.[49–53] These local estimates are then aggregated (processed) in a robust manner to provide blind estimation of noise characteristics based on a model of noise assumed known *a priori*. Pure additive or multiplicative noise variances can be blindly estimated.[49–52] More sophisticated methods allow estimating dependence of local variance on local mean for signal-dependent noise.[36,53]

The following are useful conclusions drawn from several papers:[36,49–53]

1. Accuracy of local estimates of noise variance depends on several basic factors, namely, block size, image content, true values of noise variance, spatial correlation of noise, a used method for obtaining local estimates, and its parameters.
2. Better accuracy (in terms of smaller relative errors) is provided for simpler content (less textural) images if noise variance is rather large and noise is spatially uncorrelated.
3. The appropriate block (scanning window) size is from 7×7 to 9×9 pixels[5] (i.e., 8×8 pixel blocks used in DCT-based filtering conform well with this recommendation).
4. In any case, there are normal local estimates of noise variance obtained in homogeneous image blocks that are close to true values of noise variance and abnormal estimates obtained in heterogeneous image blocks that are considerably larger than the true values of noise variance.

These conclusions indicate that it is hard to expect good accuracy of noise variance evaluation for blocks of a limited size, especially if image content in a given block is quite complex and noise is not intensive. To prove this, consider first local estimates of noise variance in spatial domain

$$\hat{\sigma}_c^2(n,m) = \sum_{q=n}^{n+7}\sum_{s=m}^{n+7} \frac{(I_{qs} - \hat{\bar{I}}_{nm})^2}{63}, \tag{6}$$

where I_{qs} is qs'th pixel value within nm'th image block and $\hat{\bar{I}}_{nm}$ denotes the nm'th block mean. It is easy to show that

$$\hat{\sigma}_c^2(n,m) \approx \mathrm{Var}\{I^{\mathrm{tr}}(n,m)\} + \sigma_n^2(n,m), \tag{7}$$

where $\mathrm{Var}\{I^{\mathrm{tr}}(n,m)\} = \sum_{q=n}^{n+7}\sum_{s=m}^{n+7}[(I_{qs}^{\mathrm{tr}} - \bar{I}_{nm}^{\mathrm{tr}})^2/63]$, $\bar{I}_{nm}^{\mathrm{tr}} = \sum_{q=n}^{n+7}\sum_{s=m}^{n+7} I_{qs}^{\mathrm{tr}}/64$, $\sigma_n^2(n,m)$ denotes the noise variance in the nm'th block. Thus, conventional estimates of local variance [Eq. (6)] are sensitive to image content in a block. It is an inherent property of such estimates, and the question is how to exploit this sensitivity in a reasonable manner. It can be a drawback or a positive feature for the considered

(a) (b) (c)

Fig. 2 (a) Noise-free test image Barbara, (b) visualized $\hat{\sigma}(n,m)$ of test image Barbara (values have been multiplied by 7) and (c) $\hat{\sigma}_c(n,m)$ (values have been multiplied by 3.5).

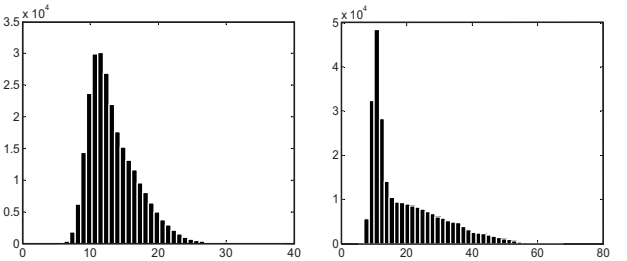

(a) (b)

Fig. 3 Histograms of (a) $\hat{\sigma}(n,m)$ and (b) $\hat{\sigma}_c(n,m)$ for the image Barbara, $\sigma_n^2=100$.

situation of unknown noise variance. The reasons will be considered next.

Let us now concentrate on estimation of noise local SD in the spectral (DCT) domain. For a given block, it is possible to estimate $\hat{\sigma}(n,m)$ in a spectral domain as[39,48]

$$\hat{\sigma}(n,m) = 1.483\ \text{med}\{|D(k,l,m,n)|: k=1,\ldots,8;\ l=1,\ldots,8;\ \text{except } k=l=1\}, \quad (8)$$

where med{ } denotes the median of a data sample. This estimate is similar to the median of absolute deviations used as a robust data scale estimator.[9] Here [in Eq. (8)], the noise SD (scale) estimate $\hat{\sigma}(n,m)$ exploits properties of transform coefficients when mixed Gaussian–Laplacian or Gaussian scale mixture models for their description are used.[54] Two properties of orthogonal transforms and robust estimation are exploited in Eq. (8). First, noise after an orthogonal transform spreads between all coefficients, and, if noise is independent identically distributed (i.i.d), its power spreads uniformly where spectral coefficients occur to be Gaussian random variables. Then, the SD of spectral coefficients is proportional to the noise SD. Second, the use of the robust estimate (median) provides less sensitivity to outliers where the outliers in the considered case are induced by image content.

However, although the used estimator (sample median) is robust, the image local content (details, texture, edges) present in a given block leads to the positive bias of the estimate $\hat{\sigma}(n,m)$.[52] Note that if noise is spatially correlated, considerable bias can be observed for estimates obtained according to Eq. (6)[51] (these estimates in homogeneous regions are, on average, smaller than the true value of noise SD).

Let us analyze how great the influence of image local content and other factors could be on accuracy of local estimates. Consider a test image [e.g., the standard test image Barbara, (Fig. 2(a))] corrupted by white additive noise with a zero mean and constant variance $\sigma_n^2=100$. The values of $\hat{\sigma}(n,m)$ from Eq. (6) are visualized in Fig. 2(b); larger values are lighter (magnification by 7 is used for better visualization). It is seen that the values $\hat{\sigma}(n,m)$ for blocks that correspond to homogeneous image regions vary a little. They are mostly rather small and approximately equal to σ_n of additive noise. The values $\hat{\sigma}(n,m)$ for the blocks that correspond to image heterogeneities such as edges, textures, and details, are commonly slightly larger due to influence of image content.

Behavior of $\hat{\sigma}_c(n,m)$ is similar [see Fig. 2(c) magnification is by 3.5], but its sensitivity to image heterogeneities in blocks is considerably larger. This can be also seen from the comparison of histograms of $\hat{\sigma}(n,m)$ and $\hat{\sigma}_c(n,m)$ presented in Figs. 3(a) and 3(b) respectively. In both cases, normal local estimates (which are obtained in homogeneous image blocks) are grouped near the true value equal to 10. But for the histogram in Fig. 3(b) there are more abnormal local estimates and they are, on average, larger.

This analysis allows proposing a locally adaptive DCT-based filter that will be further referred as LA DCT-1. This filter algorithm is as follows:

1. For each given block, estimate $\hat{\sigma}(n,m)$ according to Eq. (8) and set a local threshold as $T(n,m)=\beta\hat{\sigma}(n,m)$.
2. All other operations (DCT in blocks, thresholding, inverse DCT, and averaging for overlapping blocks) are performed as described in Section 2.

We prefer to use $\hat{\sigma}(n,m)$, but not $\hat{\sigma}_c(n,m)$, because $\hat{\sigma}(n,m)$ is less sensitive to heterogeneities. Note that the use of a larger threshold in DCT-based filtering leads to oversmoothing. As follows from the algorithm description, the proposed filter LA DCT-1 adapts to noise local characteristics. This is adaptation mechanism 1.

3.2 *Improved Locally Adaptive DCT Filter*

In this section, we consider one more way (mechanism 2) to further improve performance of the locally adaptive DCT-based filter. Our approach is based on the following general idea and assumptions. Suppose that we have succeeded in discriminating homogeneous and heterogeneous regions of an image. Because in homogeneous regions, local estimates $\hat{\sigma}(n,m)$ are quite close to true values of local SD of noise, then it is a correct decision to set the local threshold equal to $2.6\cdot\hat{\sigma}(n,m)$. On the contrary, if a given block corresponds to an image heterogeneous region, then, most probably, $\hat{\sigma}(n,m)$ is larger than the local SD of noise. Then, it is reasonable to set the local threshold less than $2.6\cdot\hat{\sigma}(n,m)$ as $\beta(n,m)\hat{\sigma}(n,m)$, where $\beta(n,m)<2.6$. In general, there are many possible ways to set $\beta(n,m)$. It can be fixed and equal to some $\beta_{\text{het}}\leqslant 2.6$ in a simplest case or it can be determined in a more complicated manner.

Thus, a primordial task is to design some discriminator for homogeneous and heterogeneous blocks. It is easy to

(a) (b)

Fig. 4 Magnified ratio image $R_{vis}(n,m)=[40R(n,m)]$ for the test image Barbara (a) corrupted by additive noise and (b) corrupted by Poisson noise.

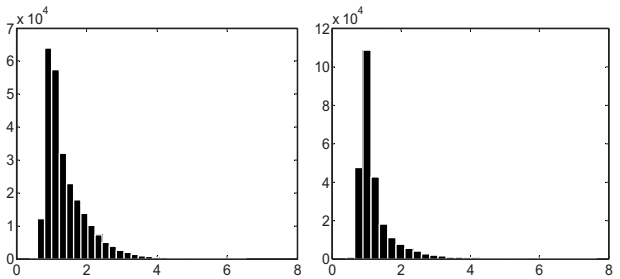

(a) (b)

Fig. 5 Histograms of the ratio $R(n,m)$ for the test images: (a) Barbara corrupted by zero mean pure additive Gaussian noise with $\sigma_n^2=100$ and (b) Lenna corrupted by Poisson noise.

resolve this task if one knows the local SD of noise in advance.[7] However, it becomes more complicated if the local SD of nonstationary noise is unknown. To get around this shortcoming, let us exploit the properties of local estimates $\hat{\sigma}(n,m)$ (in spectral domain) and $\hat{\sigma}_c(n,m)$ (in spatial domain) established in Section 3.1.

Note that usually[7] $\hat{\sigma}_c(n,m)$ is defined in square-shaped scanning windows, where window side size is odd (e.g., 5 or 7).[7,25] Because here we deal with DCT-based filtering in 8×8 blocks, it is possible to calculate $\hat{\sigma}_c(n,m)$ either according to Eq. (6) or as follows:

$$\hat{\sigma}_c^2(n,m)=\sum_{q=n+1}^{n+Q}\sum_{s=m+1}^{n+S}\frac{(I_{qs}-\hat{\bar{I}}_{qs})^2}{QS-1},$$

$$\hat{\bar{I}}_{qs}=\sum_{q=n+1}^{n+Q}\sum_{s=m+1}^{n+S}\frac{I_{qs}}{QS},\quad Q=S=6. \tag{9}$$

The map of the estimates $\hat{\sigma}_c(n,m)$ for $Q=S=6$ is visualized in Fig. 2(c) for the test image Barbara corrupted by zero mean additive noise with the constant variance $\sigma^2=100$. Because the estimate $\hat{\sigma}_c(n,m)$ is much more sensitive to image heterogeneities in a block than the estimate $\hat{\sigma}(n,m)$, let us exploit this difference for discriminating homogeneous and heterogeneous image blocks. For this purpose, consider a ratio $R(n,m)=[\hat{\sigma}_c(n,m)/\sigma(n,m)]$. Its example for the test image Barbara and additive Gaussian noise with $\sigma_n^2=100$ is visualized in Fig. 4(a). We represent the ratio map as an image $R_{vis}(n,m)=[40R(n,m)]$, $n=1,\ldots,N_{im}-7$, $m=1,\ldots,M_{im}-7$, where $[\bullet]$ means rounding to the nearest positive integer not larger than 255, $N_{im}\times M_{im}$ is the image size, 40 is a magnification coefficient used to visualize better the maps $R(n,m)$.

Joint visual analysis of the test image Barbara [Fig. 2(a)] and the ratio map [Fig. 4(a)] shows that quite large ratios (essentially larger than unity, indicated by brighter color pixels) are observed for blocks located in the heterogeneous image regions. Figure 4(b) presents the ratio map for the same test image but corrupted by Poisson noise. The obtained maps are rather similar. This indicates that the method of analyzing local activity (heterogeneity) based on $R(n,m)$ is applicable to different types of noise. This observation allows expectation that the proposed principle will also work well enough for any nonstationary noise.

There are several possible ways to exploit the aforementioned property. The simplest one is to adaptively set the local threshold

$$T(n,m)=\begin{cases}\beta\hat{\sigma}(n,m), & \text{if } R(n,m)<T_R\\ \beta_{het}\hat{\sigma}(n,m), & \text{if } R(n,m)\geq T_R\end{cases}, \tag{10}$$

where $\beta=2.6$ as in LA DCT-1, T_R is a preset threshold, $\beta_{het}<2.6$ is a factor that determines the hard threshold for DCT coefficients in edge/detail neighborhoods and in textural regions. The DCT-based filter described by Eqs. (5), (9), and (10) (further referred as to LA DCT-2) belongs to the class of locally adaptive hard-switching filters,[7] where hard switching relates to the parameter β. This filter implies both adaptions to noise characteristics (mechanism 1) and to image content (mechanism 2).

LA DCT-2 uses two new parameters, T_R and β_{het}. Consider distributions of the ratio $R(n,m)$, which is a random variable. Suppose that the estimates $\hat{\sigma}_c(n,m)$ and $\hat{\sigma}(n,m)$ are obtained in a homogeneous image region. Then, their means under condition of i.i.d. Gaussian noise are the same. Thus, it is possible to expect that the distribution of the ratio $R(n,m)$ should have a mode in the neighborhood of unity. As follows from the ratio maps in Figs. 4(a) and 4(b), $\hat{\sigma}_c(n,m)$ is usually larger than $\hat{\sigma}(n,m)$ in image heterogeneous regions. Therefore, the distribution of the ratio $R(n,m)$ may have a heavy "right-hand" tail. The histogram of the obtained $R(n,m)$ values for the test image Barbara (pure additive Gaussian noise, $\sigma_n^2=100$) is presented in Fig. 5(a). The histogram for the image Lenna corrupted by Poisson noise is shown in Fig. 5(b). Both distributions, as expected, have modes in the neighborhoods of unity, and they possess a heavy right-hand tail. Similar shapes of $R(n,m)$ value distributions have been observed for other conventional test images as Peppers, Goldhill, etc. The detailed analysis of values of these histograms shows that the distribution mode, which corresponds to homogeneous image regions, is about unity. Being random, the values $R(n,m)$ form the quasi-Gaussian part of this distribution. As in any discrimination or detection task, a larger preset discrimination threshold provides better correct detection of homogeneous regions but larger probability of recognizing heterogeneous region as homogeneous. Thus, threshold setting is

Table 1 Output MSE for "ideal" DCT-based (IdDCT) filter, LA DCT-1, and nonlinear nonadaptive filters.

Image	Lenna		Barbara		Baboon		Peppers		Goldhill	
Noise type	Gauss	Possion	Gauss	Poisson	Gauss	Poisson	Gauss	Poisson	Gauss	Poisson
IdDCT, β=2.6	19.2	19.8	23.9	25.6	59.0	67.5	22.2	23.4	30.7	31.0
LA DCT-1, β=2.6	23.7	24.1	34.0	36.1	179.5	187.5	27.2	28.2	42.5	43.4
IdDCT, β=2.3	20.6	21.3	26.0	28.0	57.9	66.5	23.3	24.8	30.9	31.6
LA DCT-1, β=2.3	21.9	23.3	29.4	31.4	147.0	155.5	25.5	26.9	37.9	38.7
Median 5×5	58.2	60.1	318.9	318.4	478.6	481.3	46.2	47.6	94.6	96.0
Median 3×3	39.7	43.6	219.5	222.8	294.5	300.6	39.4	43.4	64.9	67.1
ATM 3×3(2)	41.6	45.7	216.4	220.6	304.6	311.0	42.7	46.7	66.7	69.4
CWM 3×3(3)	38.9	44.7	127.1	112.9	169.2	177.6	38.6	43.5	52.5	56.0

a compromise. Analysis of histogram data shows that a trade-off in discriminating blocks that correspond to homogeneous and heterogeneous regions can be provided by setting $T_R \approx 1.35$.

4 Local Adaptive DCT Filter Performance Analysis

4.1 *Performance Analysis for Test Images in Case of Spatially Uncorrelated Noise*

Let us carry experiments with different types of noise and test images. Recall that if noise type and characteristics are *a priori* known, it is possible to carry out filtering in *a priori* adjusted or "ideal" manner. For example, if one knows that noise is additive with fixed σ_n^2, then it is possible to apply the standard DCT-based filter[31] with the fixed $T(n,m)=2.6\sigma_n$. Similarly, if, e.g., noise is Poissonian, filtering can be done with $T(n,m)=\beta\sqrt{\hat{I}(n,m)}$ (see Section 2). Quantitative performance characteristics for such filters that presume availability of full *a priori* information and its use, IdDCT, can serve as benchmarks of what can be reached if *a priori* information is available and is exploited in the DCT-based filtering.

Let us analyze the filter performance in conventional terms of output $\mathrm{MSE_{out}}=(1/N_{\mathrm{im}}M_{\mathrm{im}})\Sigma_{n=1}^{N_{\mathrm{im}}}\Sigma_{m=1}^{M_{\mathrm{im}}}(I_{nm}^{\mathrm{f}}-I_{nm}^{\mathrm{tr}})^2$ where MSE is mean square error, $N_{\mathrm{im}}\times M_{\mathrm{im}}$ is the image size, I_{nm}^{f} is the nm'th pixel value for the processed (filtered) image. The simulation results have been obtained for the traditional set of test gray-scale images (512×512 pixels), for Gaussian additive ($\sigma_n^2=100$) and Poisson noises. These simulation results are collected in Table 1. Two values of β have been used, namely, $\beta=2.6$ and 2.3 as motivated by dependences in Fig. 1 and analysis performed in Sections 2 and 3.

Table 1 also contains the values of $\mathrm{MSE_{out}}$ for four nonadaptive nonlinear filters: the standard median with the scanning window sizes 5×5 and 3×3 pixels, the 3×3 α-trimmed mean (ATM) filter with trimmed two largest and two smallest values in the scanning window, and the 3×3 center-weighted median (CWM) filter with the central pixel weight equal to 3.[23]

Analysis of data in Table 1 shows the following:

1. The IdDCT-based filters always perform better (produces smaller $\mathrm{MSE_{out}}$) than the proposed LA DCT-1; worse performance of LA DCT-1 is explained by inaccuracies of the used local estimates of noise SD.
2. The IdDCT-based filter with $\beta=2.6$ performs better than for $\beta=2.3$ for four considered test images; the only exception is the test image Baboon which is the most textural.
3. The difference of $\mathrm{MSE_{out}}$ for the IdDCT-based filter and LA DCT-1 for the same β is not large; the only exception is again the image Baboon. The reason is that for this image the estimates $\hat{\sigma}(n,m)$ are mostly considerably larger than the true values of local SD of noise, and this leads to oversmoothing.
4. The results for Gaussian and Poisson noise are in good agreement with each other, which is evidence that the proposed LA DCT-1 is able to carry out denoising well enough, except in the case of highly textural images.
5. The fact that for the test image Baboon both IdDCT-based filter and LA DCT-1 produce smaller $\mathrm{MSE_{out}}$ for smaller β shows that one way to improve filtering performance is to detect textural regions in images and to set smaller β for them. This idea has been put behind the method LA DCT-2 (see Section 3.2).
6. The values $\mathrm{MSE_{out}}$ for all considered nonadaptive

Table 2 Values of MSE_{out} for several β_{het} and T_R for the considered test images.

Image		Lenna		Barbara		Baboon		Peppers		Goldhill	
		Noise type									
β_{het}		Gauss	Poisson	Gauss	Poisson	Gauss	Poisson	Gauss	Poisson	Gauss	Poisson
T_R=1.37	2.6	23.7	24.1	34.0	36.1	179.5	187.8	27.2	28.2	42.5	43.4
	2.3	22.4	23.2	30.9	33.0	167.9	176.7	26.0	27.1	40.5	41.4
	2.0	21.4	22.2	28.6	30.6	156.5	165.9	24.9	26.0	38.6	39.5
	1.7	20.8	21.7	27.2	29.3	145.5	155.5	24.0	25.1	37.1	37.9
	1.4	20.9	21.8	27.3	29.4	135.5	146.1	23.5	24.6	36.0	36.9
	1.1	22.0	22.9	29.2	31.6	127.3	138.5	23.8	24.8	36.0	36.9
T_R=1.35	2.3	22.4	23.2	30.8	32.9	167.3	175.9	26.0	27.1	40.4	41.3
	2.0	21.4	22.2	28.4	30.4	155.1	164.2	24.8	25.9	38.5	39.3
	1.7	20.8	21.6	27.1	29.1	143.4	153.1	23.9	25.0	36.8	37.6
	1.4	20.9	21.8	27.1	29.3	132.8	143.1	23.5	24.5	35.8	36.6
	1.1	22.1	22.9	29.2	31.6	124.2	134.9	23.8	24.8	35.7	36.6
	0.8	24.2	25.1	33.3	36.2	118.8	129.9	25.0	26.0	36.7	37.6
T_R=1.33	2.3	22.3	23.1	30.7	32.8	166.5	175.0	26.0	27.0	40.3	41.2
	2.0	21.3	22.2	28.3	30.3	153.5	162.5	24.8	25.9	38.3	39.1
	1.7	20.7	21.6	26.9	28.9	141.0	150.6	23.8	24.9	36.6	37.4
	1.4	20.9	21.8	27.0	29.2	129.8	139.9	23.4	24.5	35.5	36.3
	1.1	22.1	23.1	29.2	31.6	120.8	131.3	23.8	24.9	35.5	36.4
	0.8	24.3	25.3	33.4	36.4	115.1	126.0	25.0	26.0	36.6	37.5
T_R=1.31	2.3	22.3	23.1	30.6	32.7	165.5	174.1	25.9	27.0	40.2	41.1
	2.0	21.3	22.1	28.1	30.2	151.6	160.7	24.7	25.8	38.1	38.9
	1.7	20.7	21.6	26.7	28.7	138.3	148.0	23.8	24.9	36.3	37.1
	1.4	20.9	21.8	26.9	29.1	126.5	136.6	23.4	24.4	35.2	36.0
	1.1	22.2	23.2	29.2	31.7	117.0	127.6	23.8	24.9	35.3	36.2
	0.8	24.6	25.6	33.6	36.7	111.1	122.1	25.1	26.1	36.5	37.4
T_R=1.29	2.3	22.3	23.1	30.6	32.6	164.6	173.1	25.9	27.0	40.1	41.0
	2.0	21.2	22.1	28.0	30.0	149.9	158.8	24.7	25.8	37.9	38.7
	1.7	20.7	21.6	26.6	28.6	135.8	145.3	23.7	24.8	36.0	36.9
	1.4	20.9	21.9	26.8	29.0	123.3	133.2	23.3	24.4	35.0	35.8
	1.1	22.3	23.3	29.2	31.7	113.3	123.7	23.8	24.9	35.1	36.0
	0.8	24.8	25.8	33.9	37.0	107.3	118.0	25.2	26.3	36.4	37.4

nonlinear filters are considerably larger than for LA DCT-1 in almost all cases; this additional time demonstrates drawbacks of these nonadaptive filters.

Concerning LA DCT-2, we have carried out numerical simulations for a set of values T_R (close to 1.35) and a set of β_{het} varied in rather wide limits. The simulation data are presented in Table 2 for the five test images corrupted by additive Gaussian noise with variance equal to 100 and Poisson noise.

As follows from analysis of the obtained results, for most images it is reasonable to set $T_R \approx 1.3$, $\beta_{\text{het}} \approx 1.5$. This choice produces falling into the neighborhood of minimal MSE_{out} for both noise models and for the four considered test images. The only exception is the test image Baboon, for which it is reasonable to use smaller β_{het}.

Reduction of MSE_{out} by approximately 10–30% is observed for LA DCT-2 in comparison to LA DCT-1 with fixed β (compare the data in Tables 1 and 2). Improvement in comparison to LA DCT-1 with fixed β is larger for more complex images. The values of MSE_{out} are almost the same as were observed for the IdDCT filter. Only for test image Baboon are the results not good enough.

We have examined the a reason for this. It occurred that the values $\hat{\sigma}(n,m)$ in image texture regions are about four times larger than the true values of local SD of noise $\hat{\sigma}(n,m)$. Thus, even if β_{het} is set to ~0.8, the local threshold is larger than $3\cdot\hat{\sigma}(n,m)$. Because of this, some oversmoothing takes place even for LA DCT-2.

In addition to hard switching of β according to Eq. (10), we have also analyzed another (soft) algorithm of threshold adaptation as follows:

$$T(n,m) = \frac{2.6\hat{\sigma}(n,m)}{R(n,m)} = \frac{2.6\hat{\sigma}(n,m)}{\hat{\sigma}_c(n,m)/\hat{\sigma}(n,m)} = \frac{2.6\hat{\sigma}^2(n,m)}{\hat{\sigma}_c(n,m)}. \tag{11}$$

We have tested this method for the same test images and noise models as presented in Table 2. Very similar results as for the LA DCT-2 with optimally set $T_R \approx 1.3$, $\beta_{\text{het}} \approx 1.5$ have been obtained. One reason why it is difficult to improve performance of the locally adaptive DCT-based filters is that there are many blocks for which the ratio $R(n,m)=[\hat{\sigma}_c(n,m)/\sigma(n,m)]$ is close to unity although these blocks are, in fact, heterogeneous. This means that, in the future, it is worth studying other local parameters than $R(n,m)$ that should be able to better discriminate homogeneous and heterogeneous image blocks. In particular, gaussianity tests in spatial or spectral domain are worth studying.[55]

Let us compare the data obtained for LA DCT-2 to other locally adaptive filters. The best known results of removing noise with *a priori* unknown characteristics are presented in the paper of Kervrann and Boulanger,[26] who perform a thorough comparison of their method to other filtering methods and demonstrate superior performance of their approach. Thus, we present our results obtained for the recommended $T_R \approx 1.3$, $\beta_{\text{het}} \approx 1.5$ and Kervrann and Boulanger's data for the same test images and noise variances (Table 3). Noise is additive white Gaussian. Filter performance is characterized by output PSNR.

Table 3 PSNR for the compared LA-DCT-2 and Kervrann's filters.

Test image	Noise SD	LA-DCT-2	Kervrann's filter	Provided PSNR
Lenna 512×512	10	35.01	Table IV in Ref. 26	35.18
Barbara 512×512	10	33.79	Table IV in Ref. 26	33.79
Peppers 256×256	10	34.32	Table IV in Ref. 26	34.07
Lenna 512×512	20	31.71	Table II in Ref. 26	32.64
Barbara 512×512	20	29.58	Table II in Ref. 26	30.37
Peppers 256×256	20	30.32	Table II in Ref. 26	30.59
Baboon 512×512	20	24.50	Figure 10 in Ref. 26	23.34

As is seen, the method[26] produces slightly better results for larger noise variance and simpler test images. In turn, our method LA DCT-2 provides larger PSNR for smaller SD of noise and more textural images. The advantage of the proposed method LA DCT-2 is that image processing is quite fast. This is due to the fact that two basic operations used in the proposed techniques are DCT and data sorting where both can be realized using fast algorithms.[42]

4.2 *Filter Performance in Spatially Correlated Noise Environment*

The case of spatially uncorrelated (i.i.d.) noise has been studied. However, in practice, it is possible that noise can be spatially correlated. Furthermore, 2-D autocorrelation function of spatially correlated noise can be unknown in advance.[7,51]

We have analyzed how the proposed LA DCT-2 filter performs in the situation of spatially correlated noise. For this purpose, we have simulated additive Gaussian zero mean spatially correlated noise with variance 100. Spatially correlated noise has been modeled by applying the 3×3 window mean filter to originally i.i.d. zero mean Gaussian 2-D noise and adjusting a desired variance. The results are presented in Table 4 for three values of T_R and several values of β_{het}. The test images are the same as earlier.

Analysis of the data presented in Table 4 shows the following:

1. For rather simple images (Lenna, Peppers, Barbara, Goldhill), there is some reduction of noise, but it is considerably smaller than in the earlier considered case of i.i.d. noise. For the image Baboon, it is still difficult to provide appropriate performance of the filter.
2. For the case of spatially correlated noise, the recommendation to set $T_R \approx 1.3$, $\beta_{\text{het}} \approx 1.5$ is incorrect. The results obtained for $T_R = 1.37$ and $\beta_{\text{het}} = 2.6$ occurred

Table 4 Values of MSE_{out} for several β_{het} and T_R for the considered test images corrupted by spatially correlated noise.

		Image				
T_R	β_{het}	Lenna	Barbara	Baboon	Peppers	Goldhill
1.37	2.6	**54.2**	**74.7**	189.5	**74.0**	**82.3**
	2.3	76.8	76.5	178.5	75.6	83.3
	2.0	79.1	78.7	167.8	77.0	84.2
	1.7	81.4	81.3	157.6	78.2	85.2
	1.4	83.8	84.1	147.7	79.3	86.2
	1.1	86.1	87.1	138.7	80.2	87.1
	0.8	88.1	89.7	131.4	81.0	88.1
1.33	2.3	76.9	76.6	177.3	75.8	83.3
	2.0	79.4	78.6	165.7	77.7	84.4
	1.7	81.9	81.6	154.6	78.8	85.5
	1.4	84.4	84.6	143.9	80.1	86.6
	1.1	86.9	87.6	134.3	81.1	87.8
	0.8	89.1	90.5	126.6	82.2	88.9
1.29	2.3	77.1	76.6	176.3	75.9	83.4
	2.0	79.7	79.1	163.6	77.7	84.6
	1.7	82.3	81.9	151.6	79.4	85.8
	1.4	85.1	85.0	140.2	80.8	87.1
	1.1	87.7	88.2	130.0	82.2	88.4
	0.8	90.1	91.2	**122.0**	83.4	89.7

to be better than for $T_R \approx 1.3$, $\beta_{het} \approx 1.5$ for four test images.

Thus, additional analysis of why it happens is needed. Some reasons are clear; they come from studies done recently.[44,56] In particular, it has been demonstrated that frequency-dependent thresholds should be used in DCT-based filter if noise is spatially correlated. Denoising with frequency-dependent thresholding can be carried out if either spatial correlation properties of noise are known in advance or preestimated. Thus, it becomes necessary to adapt not only to local statistics of noise and image local content, but also to spatial correlation characteristics of noise.

Another reason is that statistical characteristics of $\hat{\sigma}_c(n,m)$ and $\hat{\sigma}(n,m)$ as well as their ratio $R(n,m)$ change if noise is spatially correlated with respect to the i.i.d. noise case. Let us analyze histograms of $R(n,m)$ for spatially correlated noise. Two typical histograms are presented in Fig. 6. Their shapes are similar to the shapes of the histograms represented in Fig. 5. However, there is an obvious difference. The modes of the histograms in Fig. 6 occur not in the neighborhood of unity but for larger values.

This phenomenon has its explanation. For spatially correlated noise, both estimates $\hat{\sigma}_c(n,m)$ and $\hat{\sigma}(n,m)$ in homo-

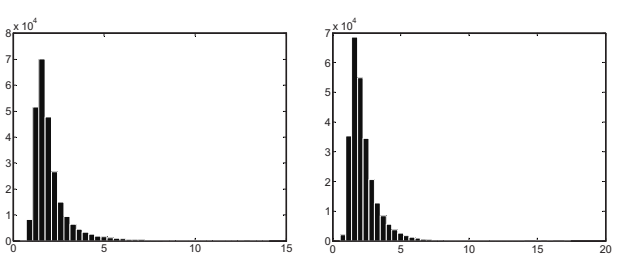

Fig. 6 Histograms of the ratio $R(n,m)$ for the test images: (a) Lenna and (b) Barbara corrupted by zero mean spatially correlated additive Gaussian noise with $\sigma_n^2 = 100$.

Table 5 Estimates $\hat{r}$ for the test images corrupted by different types of noise.

	Test image				
Noise type	Lenna	Barbara	Baboon	peppers	Goldhill
Additive white	1.006	1.034	1.141	1.000	1.047
Poisson	1.005	1.034	1.122	0.997	1.049
Additive spatially correlated	1.646	1.779	1.432	1.434	1.602

geneous blocks (that form histogram maximum) become biased, smaller than the true value of noise SD.[51] But the bias Δ_c of the estimates $\hat{\sigma}_c(n,m)$ can be about $(0.1\ldots0.2)\sigma_n^2$, whereas for the estimates $\hat{\sigma}(n,m)$ the bias Δ can reach $(0.7\ldots0.8)\sigma_n^2$.[51] Thus, the estimates $\hat{\sigma}_c(n,m)$ in image homogeneous blocks are, on average, larger than the estimates $\hat{\sigma}(n,m)$. This leads to mode shifting to values larger than unity.

Let us analyze the mode estimates $\hat{r}$ for distributions of $R(n,m)$. The obtained data are presented in Table 5. The method[49] has been applied for mode estimation.

As is seen, for spatially uncorrelated noise the estimates $\hat{r}$ are quite close to unity for all test images for both additive i.i.d. Gaussian and Poissonian noise. One interesting observation is that, for images with more complicated structure (e.g., Baboon), the estimates $\hat{r}$ are larger. Similarly, if noise is spatially correlated, the estimates $\hat{r}$ are considerably larger than 1.0 for all five considered test images.

Two conclusions follow from this analysis:

1. Practical cases when an image is either corrupted by spatially correlated noise or is textural can be discriminated from cases when an image is rather simple and corrupted by i.i.d. noise. This can be done by comparing $\hat{r}$ to some threshold T_{spc} (e.g., approximately equal to 1.15: if $\hat{r}<T_{\text{spc}}$), image filtering by LA DCT-2 can be efficient (see data in Section 4.1), whereas in the opposite case, a more complicated filtering should be applied.
2. If noise is spatially correlated, it seems reasonable to use $T_R>1.3$; adaptation to noise spatial correlation is needed.

Thus, we have determined practical situations for which the designed filter LA DCT-2 is worth applying. A decision of whether or not filtering has to be applied can be undertaken automatically by analyzing $\hat{r}$ for an image at hand. Design of adaptive DCT-based filters for complex-structure images corrupted by spatially correlated noise is a topic of future research.

5 Performance Analysis for Real-Life Images

Let us present two examples of applying the proposed filters to real-life data. One example is a set of polarimetric radar data, presented as real valued (floating point) data arrays. These data have been obtained by a maritime coastal radar. The images are presented in Fig. 7. HH means that a horizontally polarized signal is transmitted and then received; VH relates to a vertically polarized emitted and horizontally polarized received signal.

A sensed area mainly corresponds to sea surface (that occupies basic part of images and form background), one large rock (small rocky island placed in the image central part, very bright pixels), several small ones (left lower corner, groups of bright pixels), and a shadowed zone behind the large rock. The horizontal axis of images corresponds to range and vertical axis relates to azimuth of the radar. During data acquisition, internal gain control was used to partly compensate dependence of backscattered signal mean on distance.

Visual analysis of these images allows concluding that background intensity varies depending on range. More detailed analysis has been done to confirm this conclusion. First, histograms (Fig. 8) have been obtained for manually selected six "homogeneous" regions (marked by frames in images in Fig. 7) for two different sectors and three different mean distances. Analysis of sample histograms in Fig. 8 shows that the histogram shape changes with range. The distributions are asymmetric with respect to their means. There is a heavy tail to the right side from the distribution mode. Distribution modes are also different for different ranges. Outliers are seldom (occur with quite small probabilities), their values differ from the mode values by approximately ten times.

To carry out more thorough analysis, we have determined the following parameters for each image homogeneous region:

1. Minimal, maximal, and mean m_i values for each i'th fragment, $i=1,\ldots,6$
2. Variance σ_i^2 and relative variance $\sigma_{\text{rel}i}^2$ calculated as variance divided by squared mean

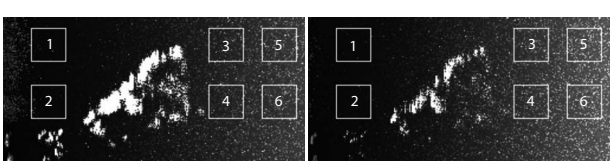

(a) (b)

Fig. 7 Data registered for (a) HH and (b) VH polarization of radar signal.

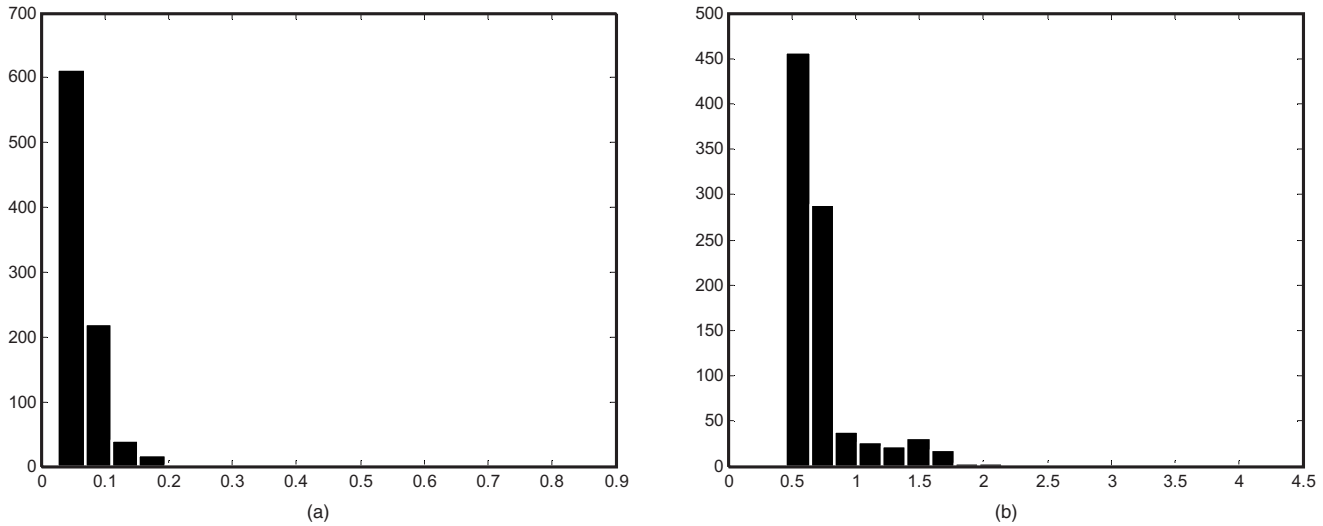

Fig. 8 Sample histograms for the image in Fig. 7(b) (a) for small distance fragment 1 and (b) for middle distance fragment 3.

3. Interquantile estimate of relative variance $\sigma^2_{\mathrm{IQ}i}$ [49] (this estimate is practically insensitive to the presence of outliers, trend, and heterogeneities in data)

The results obtained for the image in Fig. 7(a) are given in Table 6. For more distant fragments (5 and 6), the values m_i and σ_i^2 are larger than for less distant fragments, especially for the fragments 1 and 2. In turn, the standard and robust (interquantile) estimates of relative variance for more distant fragments are smaller. This shows that noise is neither pure additive nor pure multiplicative. A specific "distance-dependent" noise is observed. This conclusion has been confirmed by results of analysis carried out for the image in Fig. 7(b). The observed nonstationarity results from joint influence of several factors, namely, specific features of the receiver amplifier gain control used, varying incidence (grazing) angle of backscattering from wavy sea surface, different mutual geometry of sea wave direction and radar azimuth, etc. This is the case when it is difficult to separate the influence of these factors. We assume that nonstationary noise local statistics does not change abruptly [i.e., it is possible to consider it practically constant for fragments (blocks) of relatively small size, let us say 8 $\times$ 8 blocks commonly used in DCT-based filtering].

Table 6 Statistical characteristics of the selected "homogeneous" regions for the image in Fig. 7(a).

Fragment index	Mean	Variance	Relative variance	Interquantile estimate
1	0.056	0.0076	2.40	0.115
2	0.061	0.0094	2.54	0.152
3	0.53	0.116	0.41	0.134
4	0.52	0.067	0.24	0.126
5	0.79	0.24	0.39	0.067
6	0.77	0.13	0.23	0.081

Figure 9 presents the processed images for the maritime radar data carlier given in Fig. 8. Note that in this case, a two-stage procedure has been applied. At the first stage, the CW Median filter[23] with the 3×3 scanning window and the center element weight $W_c=5$ has been used to remove outliers. Then, at the second stage, the LA DCT-1 has been used. Comparing images in Figs. 7 and 9, one can conclude that noise is well suppressed and useful information in images is preserved well enough, although some oversmoothing of fine details is observed.

Let us give another example of a real-life image processing. The 224th subband image of the Lunar Lake AVIRIS[57–59] image is presented in Fig. 10(a). Noise present in this image is visually seen. The output image for LA DCT-1 is shown in Fig. 10(b). Noise is well suppressed, although sharp edges are slightly smeared. The ratio image $R_{\mathrm{vis}}(n,m)=[40R(n,m)]$ is visualized in Fig. 10(c). The most sharp edges and details are marked by brighter color pixels in this map. This allows better preservation of sharp edges and details in the output image by the designed LA DCT-2 [see Fig. 10(d) $T_R=1.35$, $\beta_{\mathrm{het}}=1.7$, $\hat{r}=1.03$].

6 Conclusions and Future Work

It is shown that there are practical situations where noise is nonstationary and limited *a priori* information on its statis-

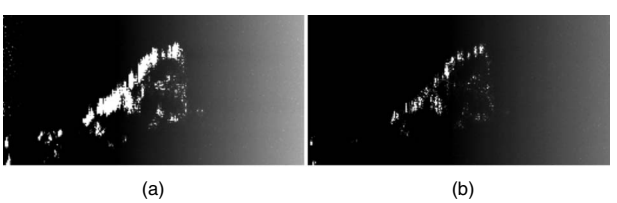

Fig. 9 Output images for (a) HH and (b) VH polarization of radar signal.

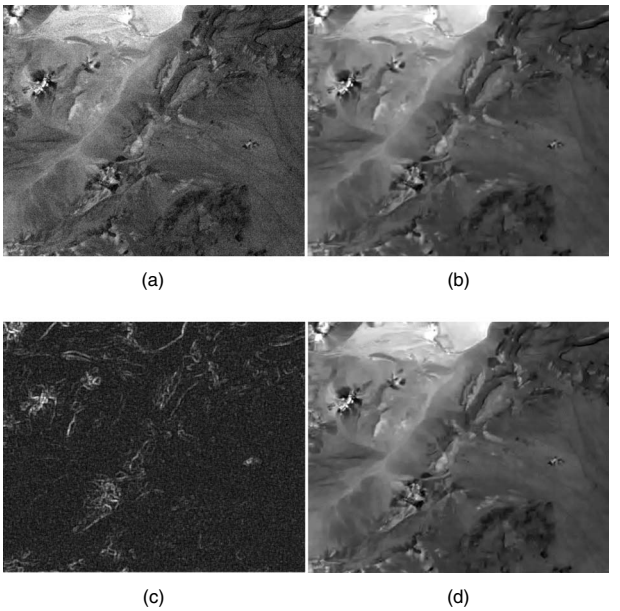

Fig. 10 (a) Original one-channel image of AVIRIS hyperspectral data, (b) the output of LA DCT-1 filter, (c) the ratio $R_{vis}(n,m)$ image, and (d) the output of the hard switching LA DCT-2 filter.

tics is available. To filter images effectively under these conditions, two DCT-based filtering techniques to suppress nonstationary spatially uncorrelated noise have been proposed and studied.

The first technique is a locally adaptive filter based on local estimation of noise variance in blocks and setting the corresponding threshold proportionally to the obtained estimate of noise SD. It performs well enough for rather simple images. The second locally adaptive filter employs, in addition, the analysis of the ratio $R(n,m)$ and adapts to image content in a block. This leads to decreasing $\mathrm{MSE}_{\mathrm{out}}$ and improving edge/detail/texture preservation in processed images. As a result, the performance of this filter is comparable to performance of the best state-of-the-art methods.

The recommendations concerning proper selection of the filter adaptation parameters are given. The designed filters have been applied to real-life images and have demonstrated excellent results. The spatially correlated noise case has been studied as well. The proposed methods do not perform well enough for this case and should be further modified. A way to discriminate the cases of spatially uncorrelated and correlated noise has been proposed. The design of locally adaptive filters for spatially correlated noise case may be a subject of our future work.

Acknowledgments

We are thankful to anonymous reviewers for their valuable comments and propositions. The work of O. Pogrebnyak was partially supported by Instituto Politecnico Nacional as a part of the research project SIP No. 20101090. Images have been kindly provided by Dr. A.V. Popov, of National Aerospace University, Kharkov, Ukraine.

References

1. P.-L. Shui, "Image denoising algorithm via doubly local wiener filtering with directional windows in wavelet domain," *IEEE Signal Process. Lett.* **12**(10), 681–684 (Oct. 2005).
2. A. Foi, V. Katkovnik, and K. Egiazarian, "Signal-dependent noise removal in point-wise shape-adaptive DCT domain with locally adaptive variance," in *Proc. of European Signal Processing Conf. (EUSIPCO 2007)*, CD-ROM, EURASIP, Poznan, Poland (2007).
3. S. Solbo and T. Eltoft, "Homomorphic wavelet-based statistical despeckling of SAR images," *IEEE Trans. Geosci. Remote Sens.* **42**(4), 711–721 (2004).
4. H.-L. Eng and K.-K. Ma, "Noise adaptive soft switching median filter," *IEEE Trans. Image Process.* **10**(2), 242–251 (2001).
5. K. Barner and G. Arce, Eds., *Nonlinear Signal and Image Processing: Theory, Methods, and Applications*, CRC Press, Boca Raton (2003).
6. K. N. Plataniotis and A. N. Venetsanopoulos, *Color Image Processing and Applications*, Springer-Verlag, New York (2000).
7. V. Melnik, "Nonlinear locally adaptive techniques for image filtering and restoration in mixed noise environments," PhD Thesis, Tampere University of Technology, Tampere, Finland (2000), ⟨http://www.atilim.edu.tr/~roktem/Research/interests.htm⟩.
8. V. V. Lukin, N. N. Ponomarenko, S. K. Abramov, B. Vozel, K. Chehdi, and J. Astola, "Filtering of radar images based on blind evaluation of noise characteristics," *Proc. SPIE* **7109**, 71090R (Sept. 2008).
9. J. Astola and P. Kuosmanen, *Fundamentals of Nonlinear Digital Filtering*, CRC Press, Boca Raton, FL (1997).
10. R. Touzi, "A review of speckle filtering in the context of estimation theory," *IEEE Trans. Geosci. Remote Sens.* **40**(11), 2392–2404 (2002).
11. D. K. Barton, *Radar System Analysis and Modeling*, Artech House, Boston (2005).
12. G. P. Kulemin, A. A. Zelensky, J. T. Astola, V. V. Lukin, K. O. Egiazarian, A. A. Kurekin, N. N. Ponomarenko, S. K. Abramov, O. V. Tsymbal, Y. A. Goroshko, and Y. V. Tarnavsky, *Methods and Algorithms for Pre-processing and Classification of Multichannel Radar Remote Sensing Images*, TTY Monistamo, Tampere, Finland (Dec. 2004).
13. C. Lopez-Martinez and E. Pottier, "On the extension of multidimensional speckle noise model from single-look to multilook SAR imagery," *IEEE Trans. Geosci. Remote Sens.* **45**(2), 305–320 (2007).
14. C.-I. Chang, Ed., *Hyperspectral Data Exploitation: Theory and Applications*, Wiley, Hoboken, NJ (2007).
15. R. Lukac, K. N. Plataniotis, B. Smolka, and A. N. Venetsanopoulos, "cDNA microarray image processing using fuzzy vector filtering framework," *J. Fuzzy Sets Syst.* **152**(1), 17–35 (May 2005).
16. G. P. Kulemin, *Millimeter-Wave Radar Targets and Clutter*, Artech House, Boston (2003).
17. C. Oliver and S. Quegan, *Understanding Synthetic Aperture Radar Images*, SciTech Publishing, Raleigh, NC (2004).
18. J. S. Lee, J. H. Wen, T. I. Ainsworth, K. S. Chen, and A. J. Chen, "Improved sigma filter for speckle filtering of SAR imagery," *IEEE Trans. Geosci. Remote Sens.* **47**(1), 202–213 (Jan. 2009).
19. A. Barducci, D. Guzzi, P. Marcoionni, and I. Pippi, "CHRIS-Proba performance evaluation: signal-to-noise ratio, instrument efficiency and data quality from acquisitions over San Rossore (Italy) test site," in *Proc. 3rd ESA CHRIS/Proba Workshop*, CD-ROM, ESA-ESRIN, Frascati, Italy (2005).
20. P. Koivisto, J. Astola, V. Lukin, V. Melnik, and O. Tsymbal, "Removing impulse bursts from images by training based filtering," *EURASIP J. Appl. Signal Process.* **2003**(3), 223–237 (2003).
21. T. Rabic, "Robust estimation approach to blind denoising," *IEEE Trans. Image Process.* **14**(11), 1755–1766 (Nov. 2005).
22. P. Huber, *Robust Statistics*, Wiley, Hoboken, NJ (1981).
23. T. Sun, M. Gabbouj, and Y. Neuvo, "Center weighted median filters: some properties and their applications in image processing," *Signal Process.* **35**(3), 213–229 (1994).
24. O. V. Tsymbal, V. V. Lukin, N. N. Ponomarenko, A. A. Zelensky, K. O. Egiazarian, and J. T. Astola, "Three-state locally adaptive texture preserving filter for radar and optical image processing," *EURASIP J. Appl. Signal Process.* **8**, 1185–1204 (May 2005).
25. L. P. Yaroslavsky, "Local criteria and local adaptive filtering in image processing: a retrospective view," in *Proc. Int. Workshop on Local and Non-Local Approximation in Image Processing (LNLA 2008)*, CD-ROM, EURASIP, Lausanne, Switzerland (2008).
26. C. Kervrann and J. Boulanger, "Local adaptivity to variable smoothness for exemplar-based image regularization and representation," *Int. J. Comput. Vis.* **79**(1), 45–69 (2008).
27. P. Perona and J. Malik, "Scale space and edge detection using anisotropic diffusion," *IEEE Trans. Pattern Anal. Mach. Intell.* **12**(7), 629–639 (1990).
28. L. Rudin, S. Osher, and E. Fatemi, "Nonlinear total variation based noise removal algorithms," *Physica D* **60**, 259–268 (1992).
29. V. G. Spokoiny, "Estimation of a function with discontinuities via local polynomial fit with an adaptive window choice," *Ann. Stat.* **26**(4), 141–170 (1998).
30. S. Mallat, *A Wavelet Tour of Signal Processing*, Academic Press, San Diego (1998).
31. V. V. Lukin, R. Oktem, N. Ponomarenko, and K. Egiazarian, "Image

filtering based on discrete cosine transform," *Telecommun. Radio Eng.* **66**(18), 1685–1701 (2007).
32. M. C. Motwani, M. C. Gadiya, R. C. Motwani, and F. C. Harris, "Survey of image denoising techniques," in *Proc. Global Signal Processing Expo and Conf. (GSPx 2004)*, CR-ROM, Global Technology Conferences, Inc., Santa Clara, CA (2004).
33. R. Oktem, K. Egiazarian, V. Lukin, N. Ponomarenko, and O. Tsymbal, "Locally adaptive DCT filtering for signal-dependent noise removal," *EURASIP J. Adv. Signal Process.* **2007**, 42472 (2007).
34. L. Klaine, B. Vozel, and K. Chehdi, "An integro differential method for adaptive filtering of additive or multiplicative noise," in *Proc. Int. Conf. on Acoustics, Speech, and Signal Processing (ICASSP 2005)*, pp. 1001–1004, IEEE, Piscataway, NJ (2005).
35. F. Argenti, G. Torricelli, and L. Alparone, "Signal dependent noise removal in the undecimated wavelet domain," in *Proc. Int. Conf. on Acoustics, Speech, and Signal Processing (ICASSP 2002)*, pp. 3293–3296, IEEE, Piscataway, NJ (2002).
36. A. Foi, "Pointwise shape-adaptive DCT image filtering and signal-dependent noise estimation," PhD Thesis, Tampere University of Technology, Tampere, Finland (Dec. 2007).
37. R. Oktem, "Transform domain algorithms for image compression and denoising," PhD Thesis, Tampere University of Technology, Tampere, Finland (2000).
38. L. Sendur and I. W. Selesnick, "Bivariate shrinkage with local variance estimation," *IEEE Signal Process. Lett.* **9**(12), 438–441 (2002); see also ⟨http://taco.poly.edu/WaveletSoftware/index.html⟩.
39. D. V. Fevralev, V. V. Lukin, A. V. Totsky, K. Egiazarian, and J. Astola, "Combined bispectrum filtering technique for signal shape estimation with DCT based adaptive filter," in *Proc. of Int. Workshop on Spectral Methods and Multirate Signal Processing (SMMSM 2006)*, CD-ROM, pp. 133–140, TICSP, Florence, Italy (2006).
40. R. Coifman and D. L. Donoho, "Translation invariant denoising," in *Wavelets and Statistics*, A. Antoniadis, Ed., Springer-Verlag, Berlin (1995).
41. D. Salomon, *Data Compression: The Complete Reference*, Springer, New York (2007).
42. L. P. Yaroslavsky, *Digital Holography and Digital Image Processing: Principles, Methods, Algorithms*, Kluwer, Dordrecht (2004).
43. H. Huang, X. Lin, S. Rahardja, and R. Yu, "A method for realizing reversible type-IV discrete cosine transform (IntDCT-IV)," in *Proc. of 7th Int. Conf. on Signal Processing (ICSP'04)*, Vol. 1, pp. 101–104, IEEE, Piscataway, NJ (2004).
44. G. Wallace, "JPEG still image compression standard," *Commun. ACM* **34**(4), 30–44 (1991).
45. A. Bovik, *Handbook on Image and Video Processing*, Academic Press, New York (2000).
46. N. Ponomarenko, V. Lukin, A. A. Zelensky, J. Astola, and K. Egiazarian, "Adaptive DCT-based filtering of images corrupted by spatially correlated noise," *Proc. SPIE* **6812**, 68120W (2008).
47. V. V. Lukin, D. V. Fevralev, S. K. Abramov, S. Peltonen, and J. Astola, "Adaptive DCT-based 1-D filtering of Poisson and mixed Poisson and impulsive noise," in *Proc. Int. Workshop on Local and Non-Local Approximation in Image Processing (LNLA 2008)*, CD-ROM, EURASIP, Lausanne, Switzerland (2008).
48. V. V. Lukin, D. V. Fevralev, N. N. Ponomarenko, O. B. Pogrebnyak, K. O. Egiazarian, and J. T. Astola, "Local adaptive filtering of images corrupted by nonstationary noise," *Proc. SPIE* **7245**, 724506 (2009).
49. V. V. Lukin, S. K. Abramov, A. A. Zelensky, J. Astola, B. Vozel, and B. Chehdi, "Improved minimal interquantile distance method for blind estimation of noise variance in images," *Proc. SPIE* **6748**, 67481I (2007).
50. V. V. Lukin, P. T. Koivisto, N. N. Ponomarenko, S. K. Abramov, and J. T. Astola, "Two-stage methods for mixed noise removal," in *Proc. EURASIP Workshop on Nonlinear Signal and Image Processing (NSIP)*, CD-ROM, EURASIP, Sapporo, Japan (2005).
51. S. Abramov, V. Lukin, B. Vozel, K. Chehdi, and J. Astola, "Segmentation-based method for blind evaluation of noise variance in images," *J. Appl. Remote Sens.* **2**, 023533 (Aug. 2008).
52. N. N. Ponomarenko, V. V. Lukin, S. K. Abramov, K. O. Egiazarian, and J. T. Astola, "Blind evaluation of additive noise variance in textured images by nonlinear processing of block DCT coefficients," *Proc. SPIE* **5014**, 178–189 (2003).
53. C. Liu, R. Szeliski, S. B. Kang, C. L. Zitnick, and W. T. Freeman, "Automatic estimation and removal of noise from a single image," *IEEE Trans. Pattern Anal. Mach. Intell.* **30**(2), 299–314 (2008).
54. J. Portilla, V. Strela, M. Wainwright, and E. P. Simoncelli, "Image denoising using Gaussian scale mixtures in the wavelet domain," *IEEE Trans. Image Process.* **12**(11), 1338–1351 (2003).
55. N. Ponomarenko, D. Fevralev, A. Roenko, S. Krivenko, V. Lukin, and I. Djurovic, "Edge detection and filtering of images corrupted by nonstationary noise using robust statistics," *Proc. 10th Int. Conf. on the Experience of Designing and Application of CAD Systems in Microelectronics (CADSM 2009)*, Polyana-Svalyava, Ukraine, pp. 129–136, IEEE (2009).
56. N. Ponomarenko, V. Lukin, I. Djurovic, and M. Simeunovic, "Prefiltering of multichannel remote sensing data for agricultural bare soil field parameter estimation," *Proc. Int. Conf. BioSense 2009*, University of Novi Sad, Novi Sad, Serbia (Oct. 2009).
57. AVIRIS Home page, ⟨http://aviris.jpl.nasa.gov/⟩ (accessed Jan 6, 2007).
58. N. Ponomarenko, V. Lukin, M. Zriakhov, and A. Kaarna, "Preliminary automatic analysis of characteristics of hyperspectral AVIRIS images," *Proc. 11th Int. Conf. on Mathematical Methods in Electromagnetic Theory (MMET 2006)*, Kharkiv, Ukraine, pp. 158–160 (2006).
59. E. Christophe, D. Leger, and C. Mailhes, "Quality criteria benchmark for hyperspectral imagery," *IEEE Trans. Geosci. Remote Sens.* **43**(9), 2103–2114 (Sept. 2005).

Vladimir V. Lukin graduated from Kharkov Aviation Institute (now National Aerospace University) in 1983, with his Diploma with honor in radio engineering. Since then he has been with the Department of Transmitters, Receivers and Signal Processing at National Aerospace University. He defended the thesis of Candidate of Technical Science in 1988 and Doctor of Technical Science in 2002 in DSP for remote sensing. Since 1995, he has been in cooperation with Tampere University of Technology. Currently, he is department vice-chairman and professor. His research interests include digital signal/image processing, remote sensing data processing, image filtering, and compression.

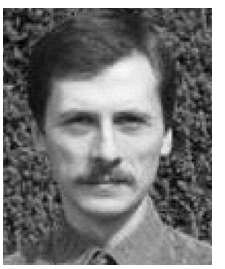

Dmitriy V. Fevralev graduated from National Aerospace University in 2002 with a Diploma in radio engineering. Since then he has been with the Department of Transmitters, Receivers and Signal Processing at National Aerospace University. He defended his thesis of Candidate of Technical Science in 2008 in DSP for bispectral analysis in radar systems. Currently, he is research fellow and part-time assistant with the Department of Transmitters, Receivers and Signal Processing. His research interests include digital signal/image processing, bispectral analysis of radar signals, and image filtering.

Nikolay N. Ponomarenko graduated from National Aerospace University in 1995 and received his Diploma with honor in computer science. Since then he has been with the Department of Transmitters, Receivers and Signal Processing at National Aerospace University. He defended his thesis of Candidate of Technical Science in 2004 in DSP for remote sensing. He also defended his thesis of Doctor of Technology at Tampere University of Technology, Finland, in 2005, on image compression. Currently, he is senior researcher and part-time associate professor with the Department of Transmitters, Receivers and Signal Processing. His research interests include digital signal/image processing, remote sensing data processing, image filtering, and compression.

Sergey K. Abramov graduated from National Aerospace University in 2000 with a Diploma with honor in radio engineering. Since then, he has been with the Department of Transmitters, Receivers and Signal Processing at National Aerospace University. He defended his thesis of Candidate of Technical Science in 2003 in DSP for remote sensing. Currently, he is associate professor and part-time senior researcher with the Department of Transmitters, Receivers and Signal Processing. His research interests include digital signal/image processing, blind estimation of noise characteristics, and image filtering.

Oleksiy Pogrebnyak received his Ph.D. degree from Kharkov Aviation Institute (now National Aerospace University), Ukraine, in 1991. Currently, he is with The Center for Computing Research of National Polytechnic Institute, Mexico. His research interests include digital signal/image filtering and compression and remote sensing.

Karen O. Egiazarian received her PhD from Moscow M. V. Lomonosov State University, Russia, in 1986, and Doctor of Technology degree from Tampere University of Technology, Finland, in 1994. He is a leading scientist in signal, image, and video processing, with about 300 refereed journal and conference articles, three book chapters, and a book published by Marcel Dekker. His main interests are in the field of multirate signal processing, image and video denoising and compression, and digital logic. He is a member of the DSP Technical Committee of the IEEE Circuits and Systems Society.

Jaakko Astola received his BS, MS, Licentiate, and PhD in mathematics from Turku University, Finland, in 1972, 1973, 1975, and 1978, respectively. From 1976 to 1977, he was with the Research Institute for Mathematical Sciences of Kyoto University, Kyoto, Japan. Since 1979 to 1987, he was with Lappeenranta University of Tecvhnology (Finland). From 1987, he is with Tampere University of Technology, Tampere, Finland. Currently, he is professor of signal processing and director of Tampere International Center for Signal Processing, academy professor by the Academy of Finland, and IEEE fellow. His research interests include signal/image processing, statistics, and image coding.